ISSN 1069-3513, Izvestiya, Physics of the Solid Earth, 2008, Vol. 44, No. 5, pp. 401–420. © Pleiades Publishing, Ltd., 2008.
Original Russian Text © D.M. Pechersky, A.F. Grachev, D.K. Nourgaliev, V.A. Tselmovich, Z.V. Sharonova, 2008, published in Fizika Zemli, 2008, No. 5, pp. 55–74.

Petromagnetic Features of Sediments at the Mesozoic–Cenozoic Boundary: Results from the Gams Section

D. M. Pechersky[a], A. F. Grachev[a], D. K. Nourgaliev[b], V. A. Tselmovich[a], and Z. V. Sharonova[a]

[a] *Schmidt Institute of Physics of the Earth (IPE), Russian Academy of Sciences, Bol'shaya Gruzinskaya ul. 10, Moscow, 123995 Russia*

[b] *Kazan State University (KSU), Kremlevskaya ul. 18, Kazan, 420008 Russia*

Received November 16, 2006

Abstract—The paper continues a cycle of petromagnetic investigations of epicontinental deposits at the Mesozoic–Cenozoic (K/T) boundary and is devoted to the study of the Gams section (Austria). Using thermomagnetic analysis, the following magnetic phases are identified: goethite (T_C = 90–150°C), hemoilmenite (T_C = 200–300°C), metallic nickel (T_C = 350–360°C), magnetite and titanomagnetite (T_C = 550–610°C), Fe–Ni alloy (T_C = 640–660°C), and metallic iron (T_C = 740–770°C). Their concentrations are determined from $M(T)$. In all samples, ensembles of magnetic grains have similar coercivity spectra and are characterized by a high coercivity. An exception is the lower coercivity of the boundary clay layer due to grains of metallic nickel and iron. With rare exceptions, the studied sediments are anisotropic and generally possess a magnetic foliation, which indicates a terrigenous accumulation of magnetic minerals. Many samples of sandy–clayey rocks have an inverse magnetic fabric associated with the presence of acicular goethite. The values of paramagnetic and diamagnetic components in the deposits are calculated. According to the results obtained, the K/T boundary is marked by a sharp increase in the concentration of Fe hydroxides. The distribution of titanomagnetite reflects its dispersal during eruptive activity, which is better expressed in the Maastrichtian and at the base of the layer **J**. The along-section distribution of metallic iron, most likely of cosmic origin, is rather uniformly chaotic. The presence of nickel, most probably of impact origin, is a particularly local phenomenon as yet. The K/T boundary is not directly related to an impact event.

PACS numbers: 91.30.Za

DOI: 10.1134/S1069351308050054

INTRODUCTION

According to numerous data, the Mesozoic–Cenozoic (K/T) boundary is fixed by an increased magnetic susceptibility of oceanic and marine deposits. Analysis of continuous sections of oceanic sediments encompassing the K/T boundary [Pechersky and Garbuzenko, 2005] showed that the K/T boundary is often (in 30% of the studied sections) marked by a peak of the magnetic susceptibility χ, although this is not its typical feature. High values of the χ peak are confined to epicenters of active plumes but are also observed far from plumes. The process of accumulation of magnetic substance in sediments can continue for from a few tens of thousands (more often) to hundreds of thousands of years. Many researchers relate the susceptibility increase to the influx of terrigenous material from continents into oceanic sediments; i.e., higher values of the magnetic susceptibility in oceanic sediments should naturally be expected near continents. However, a χ peak is often altogether absent in sedimentary cores closest to continents. Moreover, the biostratigraphic K/T boundary is not synchronous: its positions in various parts of the ocean can differ by 0.7 Myr [Pechersky and Garbuzenko, 2005]. These data indicate that the K/T boundary and the accumulation of magnetic minerals cannot be related to a single impact event.

Until recently, only the behavior of the magnetic susceptibility in sediments at boundaries of eras has been analyzed, and their other magnetic properties have not been studied. Therefore, we know virtually nothing about the nature of χ peaks at era boundaries. The relations of compositions and other characteristics of magnetic minerals in sediments to magmatic activity of plumes have not been studied at all. We attempt to compensate for these substantial drawbacks by comprehensive magnetolithologic and magnetomineralogical investigations of epicontinental deposits at the K/T boundary that are presently exposed on land and are accessible for direct studies. In particular, this paper is devoted to such a study of the Gams section (Austria). Similar investigations were undertaken in relation to the Koshak section (Mangyshlak) [Pechersky et al., 2006a], where a detailed petromagnetic study of deposits encompassing the K/T boundary was performed. As

a result, it was found that two thin clayey interbeds (one of them is located at the K/T boundary) are distinguished among the Chalk deposits by a relatively increased magnetization, which is due to a relatively higher concentration of paramagnetic minerals, Fe hydroxides (up to 0.3%), hemoilmenite (up to 0.2%), and magnetite (up to 0.01%) in these interbeds, implying that the distributions of the aforementioned magnetic, paramagnetic, and diamagnetic minerals in the sediments are controlled lithologically. Insignificant concentrations of titanomagnetite grains, apparently of volcanic origin, are found only in the Maastrichtian deposits. Rare grains of metallic iron, probably of cosmic origin, are met everywhere.

The Gams "section" in the form of a plate 6 cm thick and 46 cm high was kindly placed at our disposal for investigations by the management of the National Museum of Natural History in Vienna. The area where the plate was taken was additionally sampled by A.F. Grachev and O.A. Korchagin in a wider depth interval (±1 m around the boundary layer) [Grachev et al., 2005].

The section, belonging to the Nierntal formation, is a continuous succession of deposits including the K/T boundary [Lahodynsky, 1988; Grachev et al., 2005]. Deposits of the formation are weakly lithified and occur monoclinally. The part of the section below the K/T transition layer is represented by alternating calcareous marl and marly limestone, while clays with different amounts of calcium carbonate and interbeds enriched in quartz and/or carbonates are predominantly developed above the transition clay layer. The transition layer, enriched in the smectite component, is characterized by increased concentrations of Ir (up to 10 ppb), Cr, Co, Ni, MgO, Al_2O_3, and TiO_2. Enrichment in Fe hydroxides is noted in the lower part of the transition layer, and balls of metallic nickel are found in the upper part. The section under study is located within the reversed-polarity magnetic chron C29R [Mauritsch, 1986]. The total thickness of the C29R interval in the section is 20.5 m, and its time equivalent is 0.83 Myr [Cande and Kent, 1995]. Consequently, the average accumulation rate of sediments in the Gams section is 2.47 cm/1000 yr. On the geomagnetic polarity scale [Cande and Kent, 1995], the C29R chron occupies the interval from 65.58 to 64.75 Ma. The K/T boundary is located higher than the C29R lower boundary by 12.5 m (0.506 Myr). Consequently, the age of the K/T boundary is 65.07 Ma. The K/T boundary occupies approximately the same position in the Gubbio (Italy) [Rocchia et al., 1990] and Tetritskaro (Georgia) [Adamia et al., 1993] continuous sections.

Biostratigraphic, lithologic, geochemical, petromagnetic, and other detailed studies of the deposits of the Gams section were performed at different laboratories, both in Russia and abroad [Grachev et al., 2005]. Petromagnetic studies were carried out at the IPE Laboratory of Geomagnetism and at the Paleomagnetic Laboratory, KSU Geological Faculty. Electron microprobe analysis was performed at the Borok Geophysical Observatory.

TECHNIQUE OF PETROMAGNETIC STUDIES

The petromagnetic studies included measurements of the specific magnetic susceptibility χ, specific saturation magnetization, saturation remanence, coercivity, remanent coercivity, and A_χ and A_{rs} anisotropy. The magnetic susceptibility was measured with a KLY-2 kappabridge, and the remanent magnetization, with a JR-4 magnetometer. Hysteretic characteristics of samples were examined with the use of a coercive spectrometer [Burov et al., 1986; Yasonov et al., 1998], measuring curves of isothermal magnetization up to 0.5 T in an automatic mode. The magnetization curves were used to determine the specific saturation remanence M_{rs}, specific saturation magnetization M_s with removed paramagnetic and diamagnetic components, coercivity H_c with the removed influence of paramagnetic and diamagnetic components, and remanent coercivity H_{cr}.

The magnetization of paramagnetic and diamagnetic components was estimated from the curves of isothermal magnetization in fields exceeding the saturation field of magnetic components of samples. If the saturation field of magnetic components was not achieved, the resulting estimate of the paramagnetic magnetization can be overestimated [Richter and van der Pluijm, 1994].

The ensemble of magnetic minerals present in samples has been analyzed with the use of coercivity spectra of the normal remanent magnetization [Sholpo, 1977; Robertson and France, 1994; Egli, 2003].

The thermomagnetic analysis of rock samples was performed with the use of the Curie balance designed by Burov et al. [1986], which measures the temperature dependence of the inductive magnetization at a heating rate of 100°C/min. Such a high heating rate is attained due to the high sensitivity of the instrument, enabling the use of very small samples (less than 10 mm^3 in volume). The temperature difference across such a sample does not exceed 10°C. The thermomagnetic analysis was performed in a constant magnetic field of 200 or 500 mT. Since the saturation fields of some samples are higher than these values, we actually measured a certain inductive magnetization $M_i(T)$ that is the sum of the saturation (M_s), paramagnetic (M_p), and diamagnetic (M_d) magnetizations for such magnetic minerals as magnetite, titanomagnetite, hemoilmenite, and iron. A high magnetic saturation field is probably due to hemoilmenite grains and ferromagnetic Fe hydroxides. The $M_i(T)$ curves of the first and second heatings to 800°C were obtained for all samples.

Table 1. Magnetic properties of rocks of the Gams section

Sample no.	d, cm	χ	A_χ	J_{rs}	A_{rs}	E_{rs}	M_s	$M(800)$	$M(20)$	M_p	M_d	H_{cr}	H_c	H_{cr}/H_c	M_{rs}/M_s	MT_χ	MTM_{rs}
*t*27	93	10.9		0.442			1.89	6.9	31.8	34.3	−1.2	122	22.5	5.41	0.234		
*t*26	87	9.15		0.905			3.7	5.9	31	34.6	−3.6	109	25.1	4.33	0.245		
*t*25	82	12		1.333			4.63	5.85	28.4	31.1	−2.7	114	26.3	4.32	0.288		
*t*24	77	8.62		0.823			3.24	6.1	27.8	29.9	−2.1	112	25.9	4.34	0.254		
*t*23	72	11.7		0.962			3.74	6.4	31.3	34.3	−3	108	25.6	4.2	0.257		
*t*22	67	10.8		0.759			3.58	6.7	30.1	32.2	−2.1	107	23.8	4.48	0.212		
*t*21	62	11.1		0.865			4.89	7.3	27.6	28	−0.4	101	20	5.03	0.178		
*t*20	57	7.25		0.292			1.36	6.95	17.7	14.8	2.9	93.3	22.5	4.14	0.215		
*t*19	52	5.29		0.615			1.74	4.15	21.8	24.3	−2.5	97.2	25.3	3.84	0.353		
*t*18	47	10.8		0.594			1.95	6.75	30.9	33.3	−2.4	99.7	22.6	4.41	0.305		
*t*17	42	10.5		0.625			2.88	6.65	31.3	34	−2.7	103	22.7	4.53	0.217		
*t*16	37	12.4															
*t*16	37	3.22															
*t*15	32	10.8		0.82			3.28	6.65	30.5	32.9	−2.4	102	23.3	4.38	0.25		
*t*14	27	9.71		0.576			3.17	6.03	27.4	29.4	−2	102	18	5.65	0.176		
*W*9-1	26	13.4	1.14	1.24	1.31	1.24										*I*	*I*
*W*9-2	26	16.5		1.23	1.34	1.32	2.05										*I*
*V*9-1	24	12.5	1.08	1.14	1.32	1.31										*I*	*I*
*V*9-2	24	14.4		1.11	1.24	1.16	1.79										*I*
*t*13	23	11.6		1.01			5.63	6.8	30.3	32.4	−2.3	101	19	5.33	0.179		
*U*3-1	22	11	1.21	0.85	1.355	1.23										*N*	*N*
*U*3-2	22	11.1	1.12	0.78	1.306	1.17	3.72	0.55	26.9	35.2	−8.3	102	19.7	5.18	0.21	*N*	*N*
*U*3-3	22	9.89		0.75	1.284	1.15											*N*
*T*3-1	20	3.49		0.282	1.131	1.05	0.45									?	*N*
*T*3-2	20	3.78		0.411	1.127	1.11										?	*N*
*T*3-3	20	3.64		0.223	1.096	1.07	0.5		9.73	16.2	−6.5	93.4	35.1	2.66	0.442	?	*N*
*t*12	19	3.69															
*S*7-1	18	3.99		0.422	1.306	1.24										?	*N*
*S*7-2	18	4.15		0.463	1.173	1.17										?	*N*
*t*11	17	13.3		0.717			3.69	8.05	37.2	40.2	−3	101	19.2	5.25	0.194		
*R*2-1	16	11.7		0.4	1.186	1.12	2.06	4.23	35.1	42.5	−7.4	104	17	6.13	0.193		*N*
*R*2-2	16	11.9	1.08	0.493	1.164	1.11											*N*
*R*2-3	16	11.5	1.02	0.443	1.219	1.11	1.9										*I*
*t*10	15	12		0.694			3.3	7.5	35.3	38.3	−3	95.9	15.4	6.23	0.21		
*t*9	14.5	14.6		0.985			4.65	8.1	38.4	41.8	−3.4	101	18	5.59	0.21		
*Q*1-1	14	10.9	1.06	0.391	1.197	1.2										*I*	*I*
*Q*1-2	14	11.6	1	0.46	1.162	1.16											*I*
*t*8	13	15.7		1.112			5.4	7.9	40.4	44.8	−4.4	103	19.2	5.37	0.206		
*P*1-1	12	12.4	1.02	0.383	1.011	1.01	2.14	3.72	34.9	43	−8.1	106	15	7.1	0.179	*N*	*N*
*P*1-2	12	12.3		0.491	1.063	1.06											*I*
*t*7	11	4.07		0.354			1.05	1.8	10.9	12.5	−1.6	82.2	26.2	3.15	0.337		
*O*1-1	10	12.7		0.382	1.149	1.13	2.1	4.82	36.2	43.3	−7.1	113	17.5	6.48	0.182		*I*
*O*1-2	10	12.6		0.536	1.158	1.12											*I*
*O*1-3	10	12.1	1.03	0.514	1.148	1.09	1.69		29							*N*	*N*
*t*6	9	12.1		0.434			3.21	7.7	34.7	37.2	−2.5	93.6	13.3	7.04	0.135		
*t*5	8.5	12.8		0.478			4.18	7.9	36.2	39	−2.8	84.2	11.2	7.52	0.114		

Table 1. (Contd.)

Sample no.	d, cm	χ	A_χ	J_{rs}	A_{rs}	E_{rs}	M_s	$M(800)$	$M(20)$	M_p	M_d	H_{cr}	H_c	H_{cr}/H_c	M_{rs}/M_s	MT_χ	MTM_{rs}
*N*1-1	8	12.3		0.724	1.074	1.06										*I*	*I*
*N*1-2	8	12.3	1.05	0.63	1.175	1.03										*I*	*I*
*N*1-3	8	12.1	1.1	0.591	1.156	1.12	2.25	3.58	35.8	44.4	–8.6	118	23	5.11	0.263	*I*	*I*
*t*4	7	11.9		0.515			2.15	7.79	36.6	39.7	–3.1	108	16.7	6.48	0.24		
*M*1-1	6	12.1	1.03	0.501	1.188	1.19										*I*	*I*
*M*1-2	6	11.9		0.737	1.148	0.9	1.62									*I*	*I*
*M*6-1	6	12.4	1	0.748	1.02	0.99											*N*
*t*3	5	10.7		0.411			2.55	7.05	32.5	35.1	–2.6	103	16.9	6.09	0.161		
*L*1-1	4	10.3		0.723	1.162	1.04	3.09	3.28	29	35.5	–6.5	113	19.2	5.88	0.234		*N*
*L*2-1	4	11.2	1.07	0.694	1.166	1.07	2.56	3.25	31.8	39.3	–7.5	129	27.3	4.71	0.271	*I*	*I*
*L*8-1	4	13.4	1.02	0.698	1.2	1.19											*N*
*L*8-2	4	13.2		0.621	1.21	1.08											*N*
*T*2	3	11.9		0.559			2.83	7.3	34.8	37.9	–3.1	117	19.1	6.15	0.198		
*K*2-1	2	4.31		0.3	1.082	1.08										?	*N*
*K*2-2	2	4.02	1.09	0.347	1.013	1.01	0.53									?	*N*
*K*2-3	2	4.37		0.409	1.05	1.03										?	*N*
*K*2-4	2	5.3		0.476	1.093	0.93	1.29		13.5	18.7	–5.2	91	35.3	2.58	0.368	?	*N*
*t*1	1	6.33		0.386			1.54	3.6	19	21.2	–2.2	96.1	21.5	4.47	0.251		
Jtop	0	11		0.339		3.29	3.29	9.03	38	40	–2	67.9	9.2	7.38	0.103		
*J*6-6	1.6									24							
*J*6-5	1.2									36							
*J*6-4	0.9									32							
*J*6-3	0.6									30							
*J*6-2	0.3									49							
*J*6-1	0									60							
*J*7-1	0	15.4	1.03	0.415	1.019	0.98											*N*
*J*7-2	0	15.7		0.42	1.142	1.09	2.1										*N*
*J*3-1	0	15.5	1.04	0.676			1.65	5.5	42.6	51.1	–8.5	67.6	10.9	6.22	0.232		
*J*3-2	0	16		0.317	1.308	1.29	1.6										*N*
*J*4-1	0	15.6		0.391	1.314	1.3	1.56	7.62	44.6	50.9	–6.4	66.3	13.1	5.06	0.25		*N*
*J*4-2	0	15.6		0.302	1.311	1.27	2.01	7.72	42	47.2	–5.2	50.6	9.43	5.37	0.15		*N*
*J*5-1	0	15.1	1.04	0.407	1.289	1.19											*N*
*J*5-2	0	15.5		0.419	1.277	1.24											*N*
*I*4-1	–2	6.65	1.04	0.229	1.157	1.13	0.78									*I*	*I*
*I*4-2	–2	5.68	1.01	0.195	1.125	1.07											*I*
*I*4-3	–2	5.58															
*H*4-1	–4	5.78		0.219	1.062	1											*N*
*H*4-2	–4	5.05		0.078	1.095		0.36		14.7	21.1	–6.5	76.2	16.4	4.66	0.217		*N*
*H*6-1	–4	4.98		0.087	1.202	0.96											*N*
*H*6-2	–4	5.14	1.02	0.097	1.189	0.99										*N*	*N*
*H*6-3	–4	5.12		0.094	1.067	0.98											*N*
*k*1	–5	4.85		0.162			1.13	2.9	15.4	17.2	–1.8	87.7	13.7	6.4	0.143		
*G*3-1	–6	5.05		0.094	1.236	0.84											*N*
*G*3-2	–6	4.87		0.093	1.151	1.01											*N*
*G*3-3	–6	4.9		0.085	1.182	1	0.72										*N*
*G*6-1	–6	5.19	1.01	0.097	1.204	1.06											*N*
*G*6-2	–6	5.1		0.089	1.218	1.04											*N*
*G*6-3	–6	4.97		0.075	1.183	1.08	0.55		14.9	20.7	–5.7	97.6	13.3	7.32	0.137		*N*

Table 1. (Contd.)

Sample no.	d, cm	χ	A_χ	J_{rs}	A_{rs}	E_{rs}	M_s	$M(800)$	$M(20)$	M_p	M_d	H_{cr}	H_c	H_{cr}/H_c	M_{rs}/M_s	MT_χ	$MT\,M_{rs}$
*F*6-1	–8	4.74		0.088	1.219	1.04											*N*
*F*6-2	–8	4.68		0.089	1.245	1.04	0.66										*N*
*F*6-3	–8	4.7	1.03	0.088	1.201	1.02											*N*
*E*6-1	–10	4.64		0.072	1.224	1.03	0.68		13.6	19.1	–5.5	92.7	15.7	5.92	0.107		*N*
*E*6-2	–10	4.63		0.095	1.194	1.03											*N*
*E*6-3	–10	4.62	1.02	0.098	1.153	1											*N*
*D*6-1	–12	4.8		0.113	1.144	1	0.92		13.9	19.8	–5.9	78.3	11.8	6.64	0.123		*N*
*D*6-2	–12	4.93		0.143	1.134	1.03											*N*
*D*6-3	–12	4.19	1.03	0.124	1.15	1.03											*N*
*C*6-1	–14	5.23		0.135	1.17	0.98	0.73		14.6	20.7	–6.1	102	18	5.65	0.184		*N*
*C*6-2	–14	4.96	1.03	0.201	1.182	0.99											*N*
*C*6-3	–14	5.02		0.214	1.145	1.05											*N*
*k*2	–15	4.91		0.158			1.19	2.6	13.7	15.3	–1.6	80.8	12.6	6.41	0.133		
*B*6-1	–16	4.06	1.02	0.17	1.132	0.98											*N*
*B*6-2	–16	3.93		0.172	1.174	0.95											*N*
*B*6-3	–16	4.18		0.123	1.168	1.02	0.48	0.84	11.7	14.9	–3.3	94.7	28.2	3.35	0.254		*N*
*A*6-1	–18	4.87		0.167	1.22	1.14	0.65								0.257		*N*
*A*6-2	–18	4.62		0.16	1.12	1.04											*N*
*A*6-3	–18	4.84		0.18	1.09	1.05											*N*
*A*6-4	–18	4.76		0.184	1.17	1.13											*N*
*A*6-5	–18	4.8		0.163	1.23	1.09											*N*
*k*3	–22	4.17		0.104			0.86	2.6	13.5	15	–1.5	70.1	12.4	5.65	0.121		
*k*5/1	–33	3.67		0.119			0.62	2.1	12	13.6	–1.6	66.6	15.3	4.35	0.192		
*k*5/2	–37	3.94															
*k*6/1	–40	4.42															
*k*6/2	–45	4.95		0.103			0.9	2.9	15.5	17.4	–1.9	65.3	11.8	5.53	0.114		
*k*7/1	–48	4.55		0.083			0.82	2.7	15.1	17.1	–2	79.7	12.8	6.23	0.101		
*k*8	–52	5.72		0.11			1.02	3.7	17.6	19.2	–1.6	82.6	11.3	7.31	0.108		
*k*9/1	–54	6.68															
*k*8	–60	6.1															
*k*10/1	–63	5.48															
*k*10/2	–70	4.99		0.089			1.05	2.8	15.4	17.4	–2	77.3	10.5	7.36	0.085		
*k*10/3	–78	5.31		0.141			1.53	3.2	16.2	17.9	–2.7	87.2	10.9	8	0.092		
*k*10/4	–85	5.34		0.14			1.37	3.1	16	17.8	–1.8	85	12	7.08	0.102		
*k*11	–90	3.14															
*k*12/1	–95	6.48															
*k*12/2	–100	8.67															
*k*13	–102	3.55															
*k*14/2	–110	8.57															
*k*14/3	–115	4.93															
*k*14/4	–120	4.15		0.369			1.16	2.2	12.7	14.5	–1.8	93.1	27.4	3.4	0.318		

Note: Samples collected in 2000 and 2005 are designated by capital and lowercase letters, respectively. The value d is the along-section distance measured from the boundary layer J; χ is the specific magnetic susceptibility (10^{-9} m^3/kg); $A_\chi = \chi_{max}/\chi_{min}$ is the anisotropy of the magnetic susceptibility; M_{rs} is the specific saturation remanence (10^{-3} A m^2/kg); $A_{rs} = M_{rs_{max}}/M_{rs_{min}}$ is the anisotropy of the saturation remanence; $E_{rs} = M^2_{rs_{in}}/M_{rs_{max}} M_{rs_{min}} > 1$ and < 1 correspond to magnetic foliation and linear magnetic fabric, respectively; M_s is the specific saturation magnetization (10^{-3} A m^2/kg); $M(800)$ and $M(20)$ are magnetizations measured at 800 and 20°C; and M_p is the paramagnetic magnetization (10^{-3} A m^2/kg). Sample J6 1.7 cm in height was divided along the vertical into six pieces and M_p values for each piece are presented. M_d is the diamagnetic magnetization; H_{cr} is the remanent coercivity (mT); H_c is the coercivity (mT); MT_χ is the magnetic fabric determined from the remanent magnetization; and N and I are normal and inverse fabric, respectively.

Table 2. Results of thermomagnetic analysis of samples of the Gams section

Sample no.	*d*, cm	Fs	First heating, T_C (fraction)									Second heating, T_C (fraction)								
			Goethite	HI	Maghemite	Nickel	MT	TM	HM	Fe–Ni alloy?	Iron	Fs	HI	Nickel	MT	TM	HM	Fe	*M*(750)/*M*(20)	*M*(800)/*M*(20)
*t*27	93		120(5)		210–300					660?	740(10)		200?, 260?						0.82	
*t*26	87		120(5)		200–300		580(20)		680				200?		580				0.79	
*t*25	82		130(10)		210–300		580(20)				760?(5)				570				0.81	
*t*24	77		120(5)		220–300		590(15)		680?		745(10)				590				0.84	4.32
*t*23	72		120(10)		220–300		580(10)				760?(5)		260?		580				0.82	4.04
*t*22	67		130(10)		220–300		610(10)		670		725(5)				570		670		0.79	
*t*21	62		130(10)		230–300			590(20)			760(5)		200?			560			0.77	
*t*20	57		130(5)		210–300			610(10)								550			0.92	
*t*19	52		H		210–300			590(20)			750(10)	110?				530			0.95	
*t*18	47		130(10)		220–300			590(20)								550			0.78	
*t*17	42		130(10)		250–300			590(20)	680							560	680		0.79	
*t*15	32		130(10)		230–300		590(30)		670?						570				0.8	
*t*14	27		130(5)		200–300		580(30)		680(20)		770(10)				580				0.83	1.25
*W*9-2	26	90			300			560?(5)		630?		130	~230(40)			500			1	
*V*9-2	24		100(5)	~310(45)		360?		570(20)					~210(50)	350?		510			1	
*t*13	23		130(10)		230		590(10)		680		770?(5)				590				0.82	
*U*3-2	22	70	130(10)	260(25)			590(20)				750(10)		~210(60)		570			750		1.4
*T*3-1	20		110?(15)	240(15)	360			550(5)			760?(30)					550				
*T*3-3	20	90?					610(25)		690		760(10)	90?	210(35)		580		660?	750?		3.86
*t*12	19		140	290(20)			600(10)				745(10)									6.5
*t*11	17		130(10)		240–320		590(20)				730?(5)				590				0.77	
*R*2-1	16		150(15)	250(10)	350		590(20)	590(20)			740(5)		~200(60)		590	530	680?			2.7
*R*2-3	16		130(5)	250(15)				560(25)					~220(40)			515			0.95	
*t*10	15		150(10)		230–300			580								550			0.8	
*T*9	14.5		120(10)		240–290		570(20)				745(10)				570				0.84	
*T*8	13		150(5)		230–290		570(20)								570				0.8	
*P*1-1	12		140(10)	250(5)			590(30)						210(70)		580					1.59
*T*7	11		120(5)	200?(5)				620(10)			765(5)	90, 130	200?			540				1.29
*O*1-1	10		140(10)	210?(5)			590(40)				750(10)		~210(30)		580					1.12
*O*1-3	10		110(10)	290(10)				550(15)			730?(15)		~180(35)			535		750?	0.98	
*t*6	9		130(10)		210–330		580(20)		680?		735(10)				580				0.82	
*T*5	8.5		140(10)		240–320		600(10)		680?				H		570				0.79	
*N*1-3	8		130(10)	250(15)			590(30)						~200(40)		590		660			1.19
*t*4	7		120(10)		230–310			580?(10)								560			0.84	
*M*1-2	6		140(10)		315			565(10)			710?(5)									

Table 2. (Contd.)

Sample no.	*d*, cm	Fs	First heating, T_C (fraction)									Second heating, T_C (fraction)								
			Goethite	HI	Maghemite	Nickel	MT	TM	HM	Fe–Ni alloy?	Iron	Fs	HI	Nickel	MT	TM	HM	Fe	*M*(750)/*M*(20)	*M*(800)/*M*(20)
*M*6-1	6		120L(10)		295		570(30)				770?(15)		~190(40)		570?				0.95	
*t*3	5		130(10)		220–310		610(20)		680?						570?				0.85	
*L*1-1	4		120(15)	250(10)			585(25)				760(5)		~210(70)	450?	580			750		1.5
*L*2-1	4		150(15)	260(10)			590(25)				750(5)		~240(60)		590		670	750		1.57
*t*2	3		140(10)		220–330		580(20)				770(10)								0.84	
*K*2-4	2	90		H			590(20)				750(15)	90	~230(65)		570		660?	750		2.9
*t*1	1		130(10)	210, 280				630(10)			740?(5)	120	190, 260			520			0.94	
Jtop	0		130(10)		350					660(20)	740(10)		H			540				0.88
*J*7-2	0		120(10)		360						740?(2)		220(30)			515			1	
*J*3-1	0		140(15)		340			590(10)		650(20)	750?(5)		210(30)			550		750?		0.85
*J*3-2	0		130(10)			370		515?(5)			740?(2)		200(25)	365		515		740?		1.03
*J*4-1	0	80	150(10)		230–300			590(10)		650(20)		80	250(30)			530				0.84
*J*4-2	0	80	150(15)	250(5)	350			590(15)		650(20)			250(20)			530	650			0.9
*H*4-2	–4		110(10)					590(40)			740(20)		~250(50)			560				0.91
*k*1	–5		150(10)	210(10)	290			580(15)		660(10)	730?(5)	60	210			530			0.85	1.24
*G*6-3	–6		150(10)		200–260		590(30)				780?(5)		250(50)		570					1.08
*E*6-1	–10		150(10)		200-450			595(40)			750?(20)	60	~250(60)			540		740		1.15
*D*6-1	–12		150(10)		210		585(40)				750(20)	70			580			760		0.98
*C*6-1	–14		130(10)		200			585(40)			750?(5)	70				540		730?		1.21
*k*2	–15		130(5)		300(20)			560(15)		650(5)	760(20)	100				530		760	0.88	1.16
*B*6-3	–16		130(10)	220(15)				590(30)			760(10)		210(40)			550		750		1.22
*k*3	–22		130(10)		290(20)			610(20)	680?		735?(5)					540			0.88	
*k*5/1	–33		130(10)	210(10)	290			600(20)	660?				200?			540	660?		0.9	
k/2	–45		130(10)		210–300			600(30)			730?(5)		150			550			0.82	
*k*7/1	–48		130(5)		210–30?			590(30)				150?				550			0.82	
*k*8	–52		140(10)		210(20)			590(15)			760(10)					540			0.81	
*k*9/1	–54	80	140(10)		380		550(20)		650		765(5)									2.2
*k*10/2	–70		130(10)		300?		580(20)				760?(10)				570				0.82	
*k*10/3	–78		140(10)		210–280		580(30)								580					0.86
kO/4	–85		130(10)		210–280			590(20)			750(10)	110			550					0.84
*K*14/4	–120		140(5)	210(5)	360			620(20)			735(5)	140	200			530			1.15	

Note: Samples of the first and second collections are designated by capital and lowercase letters, respectively. *d* is the distance along the vertical from the boundary layer *J* layer, cm. T_C is the Curie point (in the case of maghemite, the temperature of transition to hematite). The fraction of magnetization (in %) determined from the curve $M_i(T)$ is given in parentheses, and the approximateness of some Curie point estimates is caused by the hyperbolic shape of the $M_i(T)$ curve, Minerals are denoted as MT (magnetite), HM (hematite), Fs (ferrospinel), HI (hemoilmenite), and TM (titanomagnetite). *M*(750)/*M*(20) and *M*(800)/*M*(20) are the ratios of magnetizations measured after 750 and 800°C heatings to their initial values.

The concentrations of magnetite, titanomagnetite, iron, hemoilmenite, and goethite in samples were estimated. For this purpose, the contribution of a given magnetic mineral to M_i was determined from the $M_i(T)$ curve, and its value was divided by the specific saturation magnetization of this mineral. According to [Nagata, 1961], the following M_s values were accepted: ~90 A m^2/kg for magnetite and titanomagnetite; ~200 A m^2/kg for iron; and 4 and 10 A m^2/kg for hemoilmenites with T_C higher than 300°C and $T_C \approx$ 250–260°C, respectively. The specific saturation magnetization of goethite varies from 0.02 to 0.5 A m^2/kg, depending on its aggregate state [Bagin et al., 1988]. For calculation of the goethite concentration, we accepted the average value $M_s = 0.25$ A m^2/kg. Judging from the ratio of the saturation magnetization M_s of all magnetic minerals present in the studied sediments to their paramagnetic magnetization M_p (Table 1), the concentration of magnetic minerals must be five to ten times smaller than the total Fe concentration (in the form Fe_2O_3) estimated from chemical analysis data. Examination of thin sections and the magnetic fraction showed that grains of ilmenite, which is paramagnetic at room temperature, are present in the samples. Therefore, the resulting estimate of the hemoilmenite concentration is the lower bound for the concentration of hemoilmenite and ilmenite in the samples studied. The obtained estimates of the concentrations of magnetic minerals are somewhat tentative, but their relative changes are authentic.

The data of magnetic measurements provide constraints on the concentrations of paramagnetic (paramagnetic Fe hydroxides, clays, etc.) and diamagnetic (carbonates and quartz) components in the sediments. The paramagnetism of samples is virtually controlled by the iron content in paramagnetic minerals. Consequently, the total iron concentration in rocks can be estimated from the paramagnetic magnetization value. If the latter is known at room temperature, the paramagnetic magnetization at 800°C can be calculated from the Curie–Weiss law. The diamagnetic magnetization is virtually independent of temperature [Vonsovskii, 1971]. Taking into account that all measurements are conducted in the same external magnetic field or reduced to one field (in this case, we assume a linear dependence of the paramagnetic and diamagnetic magnetization values on the field), the diamagnetic and paramagnetic magnetization components at room temperature can be calculated from the following simple equations:

$$M_p + M_d = M_{20},$$

$$M_p/3.644 + M_d = M_{800},$$

where M_{20} is the paramagnetic + diamagnetic magnetization determined from the curve of isothermal magnetization at room temperature above the saturation field of magnetically ordered (magnetic) minerals present in a sample, and M_{800} is the magnetization of the sample at 800°C measured in the same field. The divisor of M_p (3.644) is the ratio of temperatures 1075 K/295 K. We obtain from these equations

$$M_p = 1.378(M_{20} - M_{800}).$$

The results of these calculations are presented in Table 1.

We obtained the thermomagnetic curves during successive heatings of samples to different temperatures, which allowed us to distinguish heating-related changes that occur in samples from Curie points.

Along with the petromagnetic studies, we performed microprobe analysis of the magnetic fraction of several samples using a Camebax microanalyzer. The material of the fraction extracted by a strong permanent magnet was placed onto a conducting film with sticky layers on both sides of it; the resulting specimen had the shape of a disk 26 mm in diameter. The microprobe measurements were performed with an accelerating voltage of 20 kV and a beam current of 10 nA. The effective diameter of the probe was 2–3 μm. The concentrations of TiO_2, FeO, MgO, MnO, Cr_2O_3, Al_2O_3, SiO_2, CaO, Ni, and Cu were measured. On the whole, the results of microprobe and thermomagnetic analyses complement each other.

RESULTS OF PETROMAGNETIC STUDIES

The specific magnetic susceptibility, saturation magnetization, and saturation remanence of rocks of the Gams section vary within wide limits and generally reflect the main lithologic characteristics of rocks, such as the contributions of diamagnetic material (calcite and quartz), paramagnetic material (Fe-bearing clays and Fe hydroxides), and magnetic minerals. Therefore, the magnetization is at minimum in the Maastrichtian marls and in a series of interbeds of Danian sediments enriched in diamagnetic calcite and quartz (in particular, these are the **K** lens and the **S**, **T**, *t*-16, and *t*-19 layers). The Danian sandy–clayey deposits in a 4–25 cm interval of the section are most magnetic (Table 1, Fig. 1). In general, the patterns of the χ, M_s, and M_{rs} along-section distributions, controlled lithologically, are very similar. Against this "background," the **J** layer is sharply distinguished by its increased magnetic susceptibility but has no signatures in M_s and M_{rs}, which we explain by the fact that the main contribution to χ is made by paramagnetic material. The role of paramagnetic material, whose magnetization is 5–20 times higher than the total saturation magnetization M_s of magnetic minerals, is significant in all rocks (Table 1). The amount of paramagnetic material in the sandy–clayey deposits is about twice as large as in the marls and limestones (Table 1). A positive correlation between M_s and M_{rs} (Fig. 2a) points to a decisive role of the concentration and composition of magnetic minerals in both. Some deviations from this correlation are

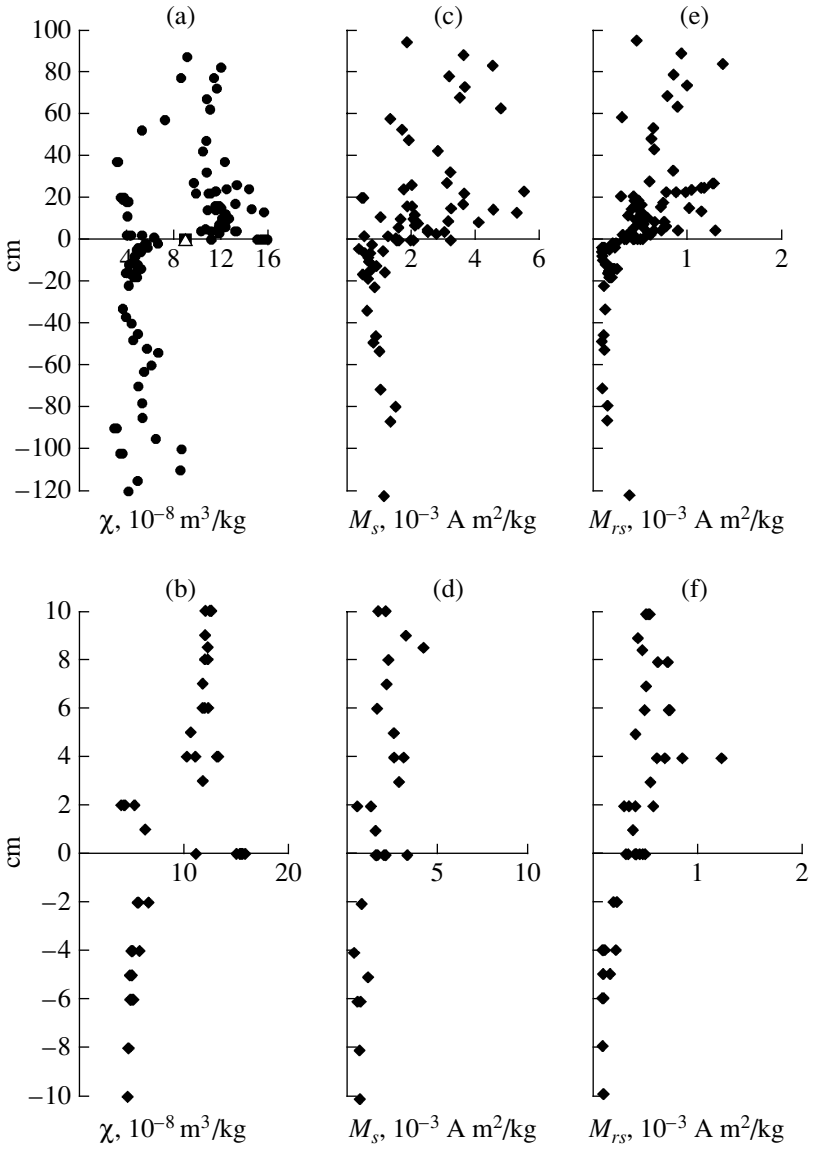

Fig. 1. Along-section distribution of (a, b) specific magnetic susceptibility χ, (c, d) specific saturation magnetization M_s, and (e, f) specific saturation remanence M_{rs}; (a, c, e) along the entire section; (b, d, f) along the ±10 cm interval. In this and other figures, the horizontal thick line marks the boundary clay layer (K/T boundary).

attributable to a significant role of structural factors (in particular, the size of magnetic grains) in M_{rs}. On the one hand, the presence of fine single-domain (SD) grains leads to underestimation of M_s compared to M_{rs}; on the other hand, the presence of superparamagnetic grains leads to overestimation of M_s compared to M_{rs}. The correlation of M_s and M_{rs} with χ is weaker (Figs. 2b, 2c), evidently because of an appreciable contribution made to the latter by paramagnetic, diamagnetic (divergences in the weakly magnetic range), and superparamagnetic (divergences in the highly magnetic range) materials, whose effects are mostly eliminated in M_s and absent in M_{rs}. The points of the M_s versus χ diagram in Fig. 2b form two groups: the first reflects the correlation between these characteristics due to an appreciable contribution of magnetic minerals to the susceptibility, and no correlation is observed in the second group, which can be due to the fact that only paramagnetic materials contribute to the susceptibility. All points of the second group are obtained solely from the Danian sandy–clayey deposits (Table 1). A strong positive correlation between χ and M_p indicates that the susceptibility is associated with paramagnetic material (Fig. 2d).

Composition of magnetic minerals. Analysis of the $M_i(T)$ curves and their derivatives revealed the presence of the following nine magnetic phases [Pechersky et al., 2006b].

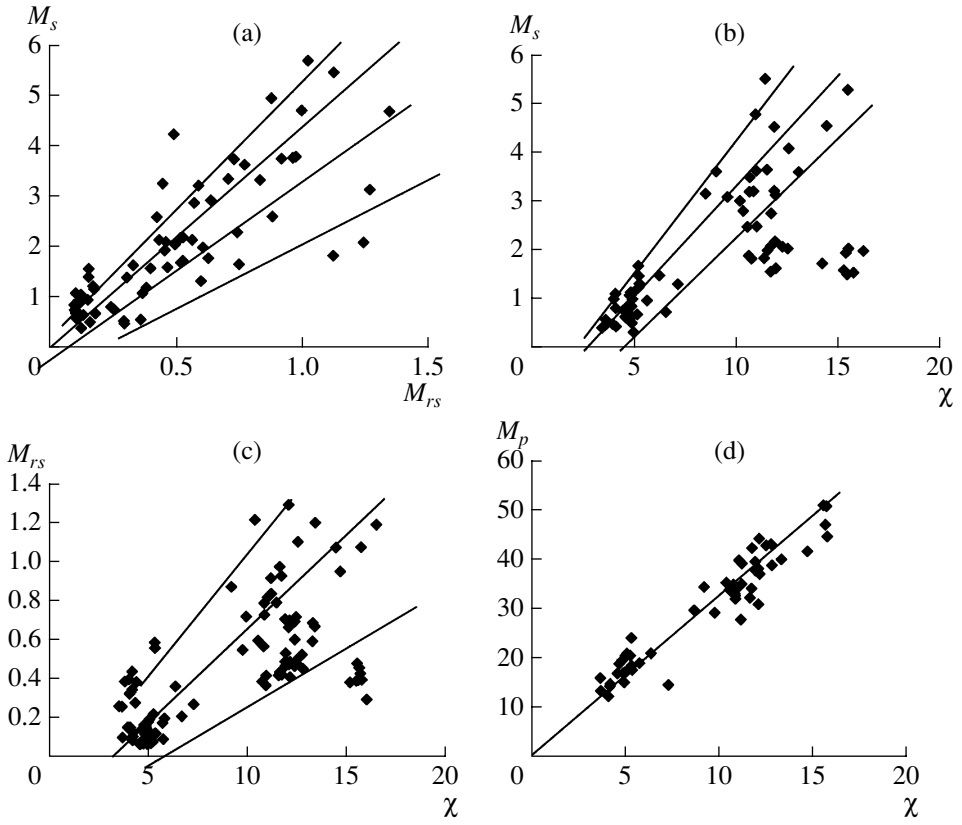

Fig. 2. Correlation between (a) M_{rs} and M_s, (b) M_s and χ, (c) M_{rs} and χ, and (d) M_p and χ.

(1) T_C **= 60–140°C.** This magnetic phase is masked in the first heating curves of the thermomagnetic analysis (TMA) by magnetic hydroxides (goethite) and the hyperbolic shape of the TMA curve; it is better seen in differential TMA curves, particularly those of secondary heating. The contribution of this phase to M_i does not exceed 10%. The phase is stable during heating to 800°C and probably arises as a result of such heating. This is possibly ferrospinel fixed in a number of experiments [Bagin et al., 1976, 1977; Gapeev et al., 1986; Lykov and Pechersky, 1976, 1977]. No relation of this mineral to lithologic characteristics or mineral composition has been noted (Table 2).

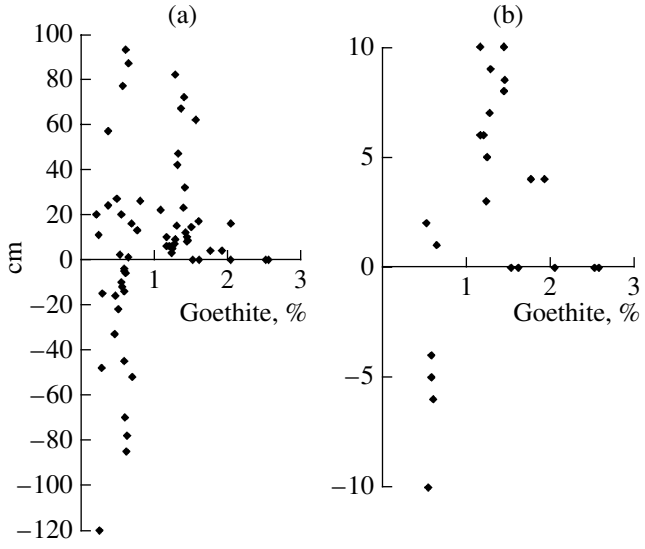

Fig. 3. Goethite concentration determined from data of thermomagnetic analysis: (a) along the entire section; (b) in the ±10 cm interval.

(2) T_C **= 90–150°C.** This phase is present in all samples under study, and its contribution to M_i is 10–20% (Table 2). After heating, this phase disappears. Most likely, it consists of Fe hydroxides of the goethite type. If we assume that this phase is goethite with M_s = 0.25 A m^2/kg, its concentration should vary from 0.2–0.6% in the Maastrichtian marls, **K** lens, and weakly magnetic interbeds of the Danian sediments to 1–2.5% in the sandy–clayey sediments, attaining a maximum (2.5%) in the boundary layer **J** (Fig. 3).

(3) T_C **= 180–300°C.** This phase is present in samples collected near the boundary layer **J** (±20 cm). Its contribution to M_i is 0–40% (Table 2). Upon heating to 800°C, the fraction of this phase in many samples increases to 30–90% (an appreciable increase in magnetization) and the Curie point often decreases (Table 2). After heating of the samples to 750°C, the magnetization does not increase. This is supported by successive heatings of samples (e.g., K2-4, Fig. 4). Judging from

an increase in M_i with decreasing T_C, this phase is hemoilmenite. During heating, it partially homogenizes, which results in a noticeably convex shape of the curve $M_i(T)$. The control heating of some samples to 1000°C removes the convexity of this curve, and the $M_i(T)$ value additionally increases by two to three times as compared with the results of heating to 800°C (Fig. 5). This corresponds to the diagram of state of hemoilmenite of an intermediate composition whose range of homogeneous states lies above 900°C [Nagata, 1961]. The hemoilmenite concentration varies from <0.0001 to 0.08% (Fig. 6). Large amounts of ilmenite grains (fragments) are present in magnetic fractions of all samples examined with the microprobe. The grains often have the shape of relatively large (more than 50 μm) plates. Their concentration in the sediments is from a few tenths of percent to a few percent, and they are close in composition to pure ilmenite (Table 3). None of hemoilmenite grains has a composition corresponding to a Curie point of 200–300°C. Evidently, the majority of hemoilmenite grains are very fine, smaller than the probe size, which is indicated by their high coercivity, and the concentration of hemoilmenite with T_C = 180–300°C is one to two orders of magnitude lower than the concentration of ilmenite. Very thin lamellae of hemoilmenite similar to hematite (tenths or hundredths of a micrometer) are recognizable in ilmenite grains. Their composition cannot be measured with a probe 2–3 μm in size. However, their presence is confirmed by the fact that ilmenite is well extracted by a magnet, apparently due to hemoilmenite inclusions, because pure ilmenite at room temperature is paramagnetic. Thus, the along-section distribution of hemoilmenite reflects the degree of heterophase oxidation of ilmenite rather than its total concentration.

Mg–Al ferrospinels with similar Curie points (200–300°C) can also form during laboratory heatings. To obtain this phase, Fe-, Mg-, and Al-bearing silicates decomposing at high temperatures must be present in rocks [Bagin et al., 1976, 1977; Gapeev et al., 1986]. However, there is no correlation between the amount of this magnetic phase and the Fe, Mg, and Al concentrations [Grachev et al., 2005]. Thermomagnetic analysis of the magnetic fraction extracted by a permanent magnet and the nonmagnetic residue from samples collected from the **L** and **W** layers provides another argument: as seen from Fig. 7a, the phase with a Curie point of about 250°C is fixed precisely in the magnetic fraction. The curves $M_i(T)$ of the second and third heatings lie well below the curve of the first heating because nearly half of magnetite disappears, apparently due to its oxidation to hematite during heating. The largest amount of Mg–Al ferrospinels might be expected to form from the nonmagnetic fraction, but its heatings do not lead to any changes (Fig. 7b).

(4) $\boldsymbol{T_C}$ **= 200–370°C.** This magnetic phase is observed in most samples of the section and, as seen from data of successive heatings, is destroyed upon heating to 300°C (Table 2); i.e., in the vast majority of cases, this is not a Curie point but the ordinary process of maghemite-to-hematite transformation.

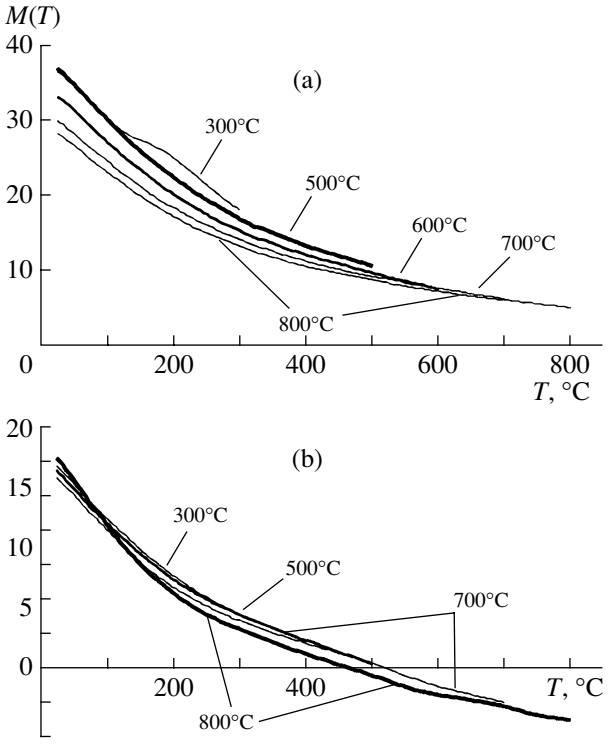

Fig. 4. Results of successive heatings of samples J3-1 (a) and K2-4 (b).

(5) $\boldsymbol{T_C}$ **= 360°C.** This magnetic phase is discovered in samples from the **J** layer (samples J6-4, J6-6, and J3-2). The microprobe analysis revealed metallic nickel in sample J6-6 from the upper part of the **J** layer and in sample J6-4 from its middle part (in two fragments less than 3 mm in size) [Grachev et al., 2005]. In all remaining samples of the section, including samples J6-1, 2, 3, and 5, metallic nickel was not detected from the curves $M_i(T)$ (Table 2). The average concentration of nickel grains in the **J** layer is apparently less than 0.001% (~0.01, ~0.1, and ~0.02% in small fragments from samples J6-4, J6-6, and J3-2, respectively). The detection of metallic nickel only in a few tiny specimens points to its local and very nonuniform distribution in the **J** layer. Apart from the **J** layer, the microprobe detected an intergrowth of pure nickel and copper in sample **L**6. The thermomagnetic analysis did not reveal nickel in the **L** layer, which confirms its extremely nonuniform distribution. The presence of a few nickel grains in the **L** layer possibly results from denudation of the uppermost part of the **J** layer and redeposition of nickel particles that precipitated mainly during the sedimentation of the uppermost part of the **J** layer.

(6) $\boldsymbol{T_C}$ **= 510–610°C.** This magnetic phase is present in all studied samples of the section, and its contribution to M_i varies from 5 to 40% (Table 2). This phase is,

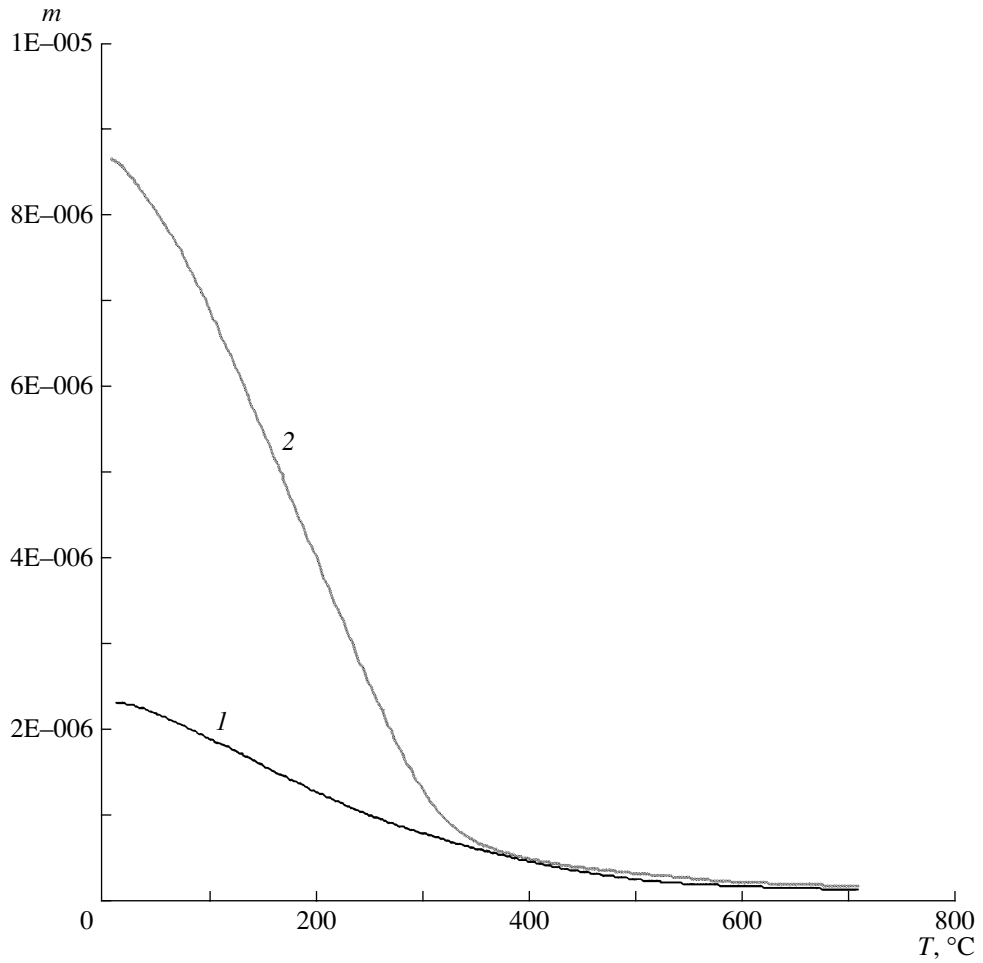

Fig. 5. Results of thermomagnetic analysis of a sample from the layer **L** after its heating to (*1*) 800°C (20 min) and (*2*) 1000°C (20 min). *m* is the magnetic moment (10^{-6} A m^2).

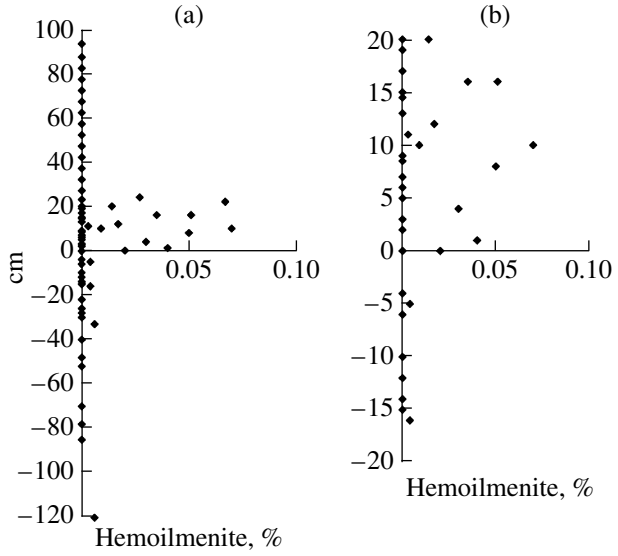

Fig. 6. Hemoilmenite concentration determined from data of thermomagnetic analysis: (a) along the entire section; (b) in the ±20 cm interval.

Table 3. Composition of minerals from magnetic fractions of sediments of the Gams section (data of microprobe analysis)

Sample, mineral	TiO_2	FeO	MgO	MnO	Al_2O_3	Cr_2O_3	Grain size, μm
L6, pt.1, ilmenite	40.2	51.9	0.9	0.1	0.3	0.0	20 × 20
pt.2, ilmenite	45.4	52.9	0.8	0.0	0.2	0.1	50 × 60
pt.3, ilmenite	46.1	52.2	0.6	0.1	0.2	0.1	10 × 10
pt.4, ilmenite	40.5	56.6	0.4	0.0	0.6	0.1	10 × 15
pt.5, ilmenite	45.5	51.2	0.2	0.0	0.2	0.1	20 × 25
pt.6, ilmenite	44.5	53.2	0.1	0.1	0.2	0.2	20 × 30
pt.7, magnetite	0.0	93.8	0.1	0.2	0.1	0.0	30 × 30
pt.8, magnetite	0.0	93.8	0.2	0.1	0.1	0.1	20 × 20
L7, pt.1, magnetite	0.0	93.9	0.0	0.0	0.5	0.1	15 × 15
pt.2, ilmenite	47.4	50.2	0.5	0.1	0.2	0.0	10 × 10
pt.4, ilmenite–rutile	81.0	15.9	0.0	0.0	0.3	0.0	10 × 25
M4, pt.1, magnetite	0.0	93.1	0.0	0.1	0.1	0.0	40 × 40
pt.2, magnetite	0.0	95.2	0.0	0.2	0.2	0.0	50 × 50
pt.3, ilmenite	47.2	51.2	0.2	0.1	0.2	0.1	20 × 20
pt.4, magnetite	0.0	93.9	0.1	0.1	0.1	0.0	50 × 50
pt.5, magnetite with clay	0.0	82.8	0.9	0.3	2.2	0.1	6 × 6
pt.6, magnetite with clay	0.0	84.6	2.2	0.3	3.0	0.1	10 × 20
O4/5, pt.1, magnetite	0.0	94.1	0.0	0.0	0.2	0.1	20 × 20
pt.2, magnetite	0.0	95.2	0.0	0.2	0.2	0.0	30 × 30
pt.3, ilmenite	46.1	52.2	0.6	0.2	0.2	0.0	10 × 10
pt.4, ilmenite–rutile	80.5	17.9	0.0	0.0	0.3	0.0	10 × 20
pt.5, magnetite	0.0	93.6	0.0	0.1	0.1	0.1	30 × 30
pt.6, magnetite with clay	0.0	88.8	0.7	0.1	0.2	0.1	4 × 4
pt.7, magnetite	0.0	94.6	0.2	0.0	0.2	0.1	40 × 50
pt.8, ilmenite–rutile	82.4	14.2	0.2	0.0	0.1	0.2	20 × 30
pt.8a, rutile lamellae	94.5	0.0	0.0	0.0	0.1	0.1	
P5, 6, pt.1, ilmenite	46.0	53.9	0.1	0.0	0.2	0.0	20 × 25
pt.2, magnetite	0.0	94.2	0.2	0.1	0.1	0.0	25 × 25
pt.3, magnetite	0.0	93.9	0.0	0.2	0.3	0.1	25 × 25
pt.4, rutile	98.8	0.6	0.1	0.1	0.1	0.0	10 × 25
pt.4a, ilmenite	45.4	49.2	0.2	0.1	0.5	0.1	3 × 5
W, upper part							
pt.1, ilmenite	43.0	54.9	0.1	0.0	0.1	0.0	10 × 10
pt.2, ilmenite	45.2	47.2	0.2	0.1	0.6	0.1	15 × 15
pt.3, rutile	98.8	0.6	0.1	0.1	0.1	0.0	10 × 25
W, lower part							
pt.4, ilmenite	45.5	53.9	0.0	0.0	0.3	0.0	20 × 20
pt.5, ilmenite	46.3	49.2	0.1	0.1	0.4	0.1	15 × 15
pt.6, rutile	96.8	1.6	0.0	0.0	0.0	0.0	10 × 25

as a rule, preserved after heating, but its amount usually decreases and, in some samples, T_C shifts toward lower temperatures. This is titanomagnetite transformed into magnetite due to heterophase oxidation; magnetite in turn often experiences single-phase oxidation ($T_C > 580$°C). As a result of laboratory heating to 800°C, titanomagnetite grains partially homogenize and T_C shifts toward lower temperatures. This feature is possible evidence for the presence of titanomagnetite in many samples of the section; its concentration varies

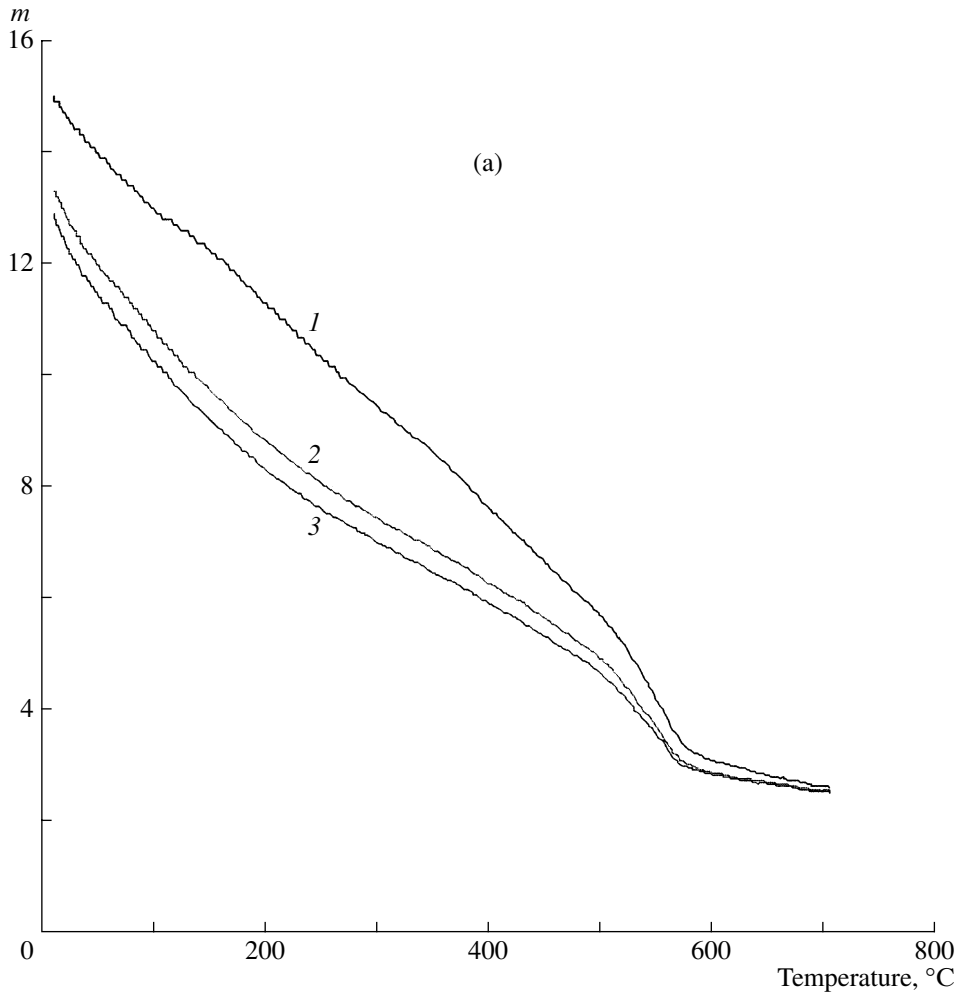

Fig. 7. Results of the first, second, and third heatings of a sample from the layer **W**: (a) magnetic fraction of the sample; (b) nonmagnetic residue. m is the magnetic moment (10^{-7} A m^2).

mainly from 0.001 to 0.01%, and its distribution does not depend on the rock composition (Fig. 8). The presence of titanomagnetite in the **J** layer is confirmed by data of microprobe analysis: its grains are close in composition to titanomagnetites typical of basalts (~20–25%TiO_2) [Grachev et al., 2005]. As distinct from titanomagnetite, magnetite is subject to lithologic control, and its concentration increases from zero in the **J** layer to 0.017% in the **O** layer (Fig. 8). The absence of titanomagnetite in this interval is confirmed by microprobe data: only magnetite that does not contain titanium is discovered in the **K**, **L**, **M**, **O**, and **P** layers (Table 3). There is no correlation between the presence of titanomagnetite and the concentration of magnetite and titanomagnetite; i.e., their sources are different (Fig. 8). Well-preserved single crystals are very often met among magnetite fragments in magnetic fractions, which points to a nearby provenance or in situ crystallization of magnetite. Such crystals of pure magnetite are evidently of nonmagmatic origin. The amount of magnetite in samples from the **K** and **T** layers increases upon heating, which is accompanied by a more than threefold increase in M_i (Table 2).

(7) $\boldsymbol{T_C}$ **= 650–660°C.** This phase is reliably fixed in samples from the **J** layer (Table 2) and is possibly present in samples t14 (27 cm), k1 (–5 cm), and k2 (–15 cm). The contribution of this phase to M_i is 5–20%. Upon heating to 800°C, this phase almost completely disappears; i.e., it is not hematite. Given that nickel is present in samples of the **J** layer, we may suggest that this phase is an alloy of iron and nickel. A simple calculation with the use of the T_C and M_s values of iron and nickel shows that possibly this is Fe_3Ni, which is confirmed by microprobe data [Grachev et al., 2005]; its concentration is about 0.005%.

(8) $\boldsymbol{T_C}$ **= 660–680°C.** This phase forms, exists, and is preserved in some samples upon heating to 800°C (Table 2). This is evidently hematite. Its contribution to M_s is usually less than 10%.

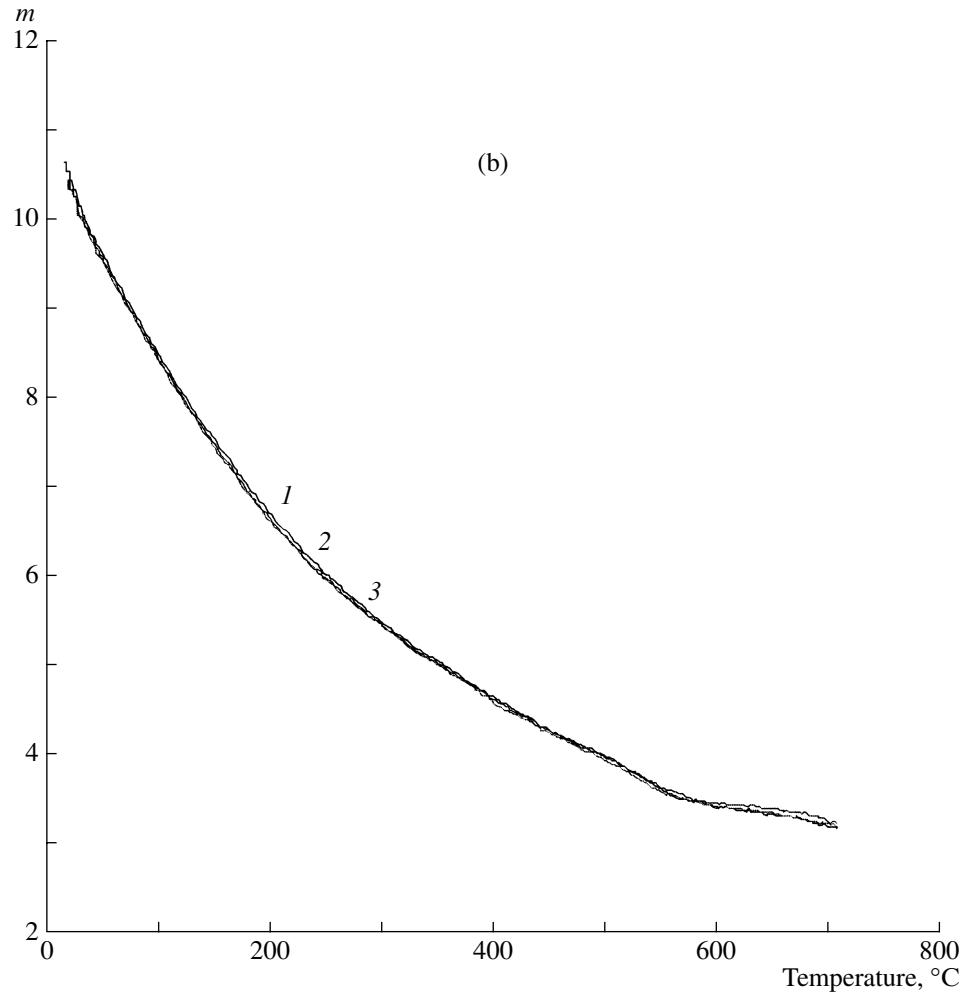

Fig. 7. (Contd.)

(9) T_C **= 740–770°C.** This phase is present in many samples, and its contribution to M_i is 0–30% (Table 2). Upon heating to 800°C, it partially or completely disappears. Evidently, this phase is metallic iron with minor admixtures that oxidizes upon heating to 800°C. A few balls of pure iron are detected with the microprobe in samples J2 and M4 [Grachev et al., 2005]; its concentration is less than 0.002%. The along-section distribution of metallic iron is rather uniform (Fig. 9).

Coercivity of magnetic minerals. As seen from coercivity spectra [Pechersky et al., 2006b], ensembles of magnetic grains are similar in all samples except samples from the **J** layer. The coercivity spectra reveal a smooth increase to a maximum at 100–140 mT, followed by a drop to a minimum at ~400 mT with a subsequent rise to 500 mT. Against this background, the coercivity spectra of **J** samples are sharply distinguished by a maximum or a flat inflection in the low coercivity range at 25–40 mT. In the remaining part, their spectra are similar to those of samples of the sandy–clayey deposits.

There is no correlation of the coercivity of rocks with the concentration and composition of rocks and minerals (Table 1; Figs. 3, 6, 8, 9); only a general tendency toward a concurrent increase in the coercivity and goethite concentration in rocks can be noted. Consequently, the coercivity of rocks is primarily controlled by the structural state of magnetic grains rather than by their composition and concentration. The coercivity drop in the **J** layer is clearly seen from both H_{cr} (Table 1) and the coercivity spectrum.

Judging from the H_{cr} and M_{rs}/M_s values (Table 1), coarser pseudo-single-domain (close to multidomain) magnetic grains prevail in the Maastrichtian limestones, whereas hard fine SD grains (and close to them in size) are distributed in the sandy–clayey deposits. The finest SD magnetic grains are present in the **K** lens and **T** layer. The smallest value of H_{cr} in samples from the **J** layer (Table 1) has no signatures in M_{rs}/M_s and H_{cr}/H_c, which confirms that H_{cr} is unrelated to the size of magnetic grains and is controlled by the presence of magnetically soft nickel.

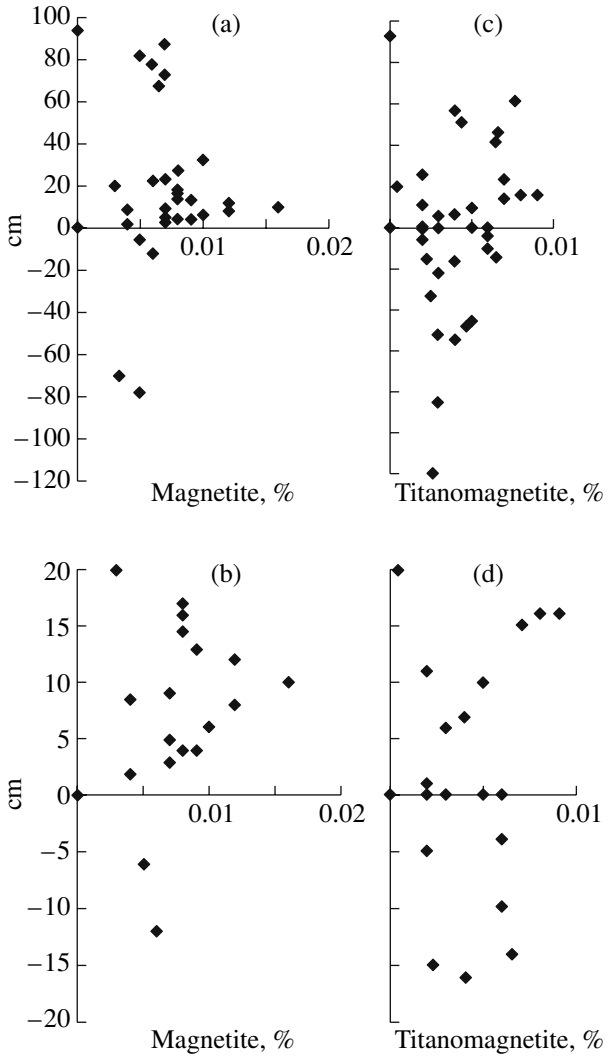

Fig. 8. Concentrations of (a, b) magnetite and (c, d) titanomagnetite determined from data of thermomagnetic analysis: (a, c) along the entire section; (b, d) in the ±20 cm interval.

Anisotropy. The anisotropy of the magnetic susceptibility (A_χ) and saturation remanence (A_{rs}) was measured. The A_χ values of the main group lie within 1–1.1, and only four samples have $A_\chi > 1.1$, whereas the A_{rs} values of this group lie within 1.12–1.36 and only four samples have $A_\chi \le 1.11$ (Table 1). Apparently, this is due to the fact that the paramagnetic and diamagnetic parts of the studied sediments are generally isotropic, and the distributions of their symmetry axes are nearly chaotic, although calcite and clayey minerals are anisotropic (A_χ is 1.13 for calcite and 1.2–1.35 for clays; quartz is isotropic [Rochette et al., 1992]). In the layers from **A** to **R**, the anisotropy A_{rs} varies within similar limits. An exception is the boundary clay interbed, where the anisotropy has a large scatter (from 1.02 to 1.32).

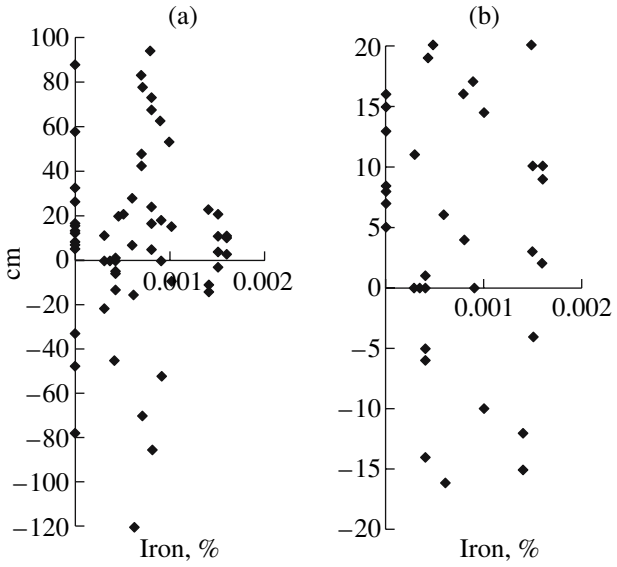

Fig. 9. Concentration of metallic iron determined from data of thermomagnetic analysis: (a) along the entire section; (b) in the ±20 cm interval.

The vast majority of sediments of the section have a magnetic foliation ($E = M^2_{rs_{in}}/M_{rs_{max}} x M_{rs_{min}} > 1$), and only some horizons are characterized by either $E \sim 1$ or very weak linearity (the **B**, **C**, **G**, and **H** samples of the Maastrichtian section interval) (Table 1). All the aforesaid can be accounted for by the presence of elongated grains of magnetic minerals, compaction of the sediments, a certain role of flows, etc. The presence of anisotropy and a magnetic fabric points to the terrigenous origin of the accumulation of magnetic minerals.

Apart from the normal magnetic fabric, with the *minimum* susceptibility perpendicular to the bedding plane, there are present intervals of an inverse fabric, with the *maximum* susceptibility perpendicular to the bedding plane (the **I**, **L**, **M**, **N**, **O**, **P**, **Q**, **V**, and **W** horizons). Samples with the normal fabric are also met in these horizons (Table 1). Such an inverse magnetic fabric is inherent in acicular goethite, whose easy magnetization axis is perpendicular to the axis of grain elongation [Rochette et al., 1992; Bagin et al., 1988]. The magnetic anisotropy value and specific features of the magnetic fabric do not correlate with the composition and concentration of magnetic minerals, but the following general tendency is noted: only the normal magnetic fabric characterizes the marls, where the goethite concentration is much lower than in the sandy–clayey sediments (Table 1); therefore, the inverse fabric is evidently associated with the presence of acicular goethite.

Paramagnetic magnetization. The paramagnetic magnetization is actually controlled by the total iron content in rocks, as is seen from the positive correlation of this magnetization, first, with the total iron concentration in rocks obtained from chemical analysis data; second, with the goethite concentration; and, third, with

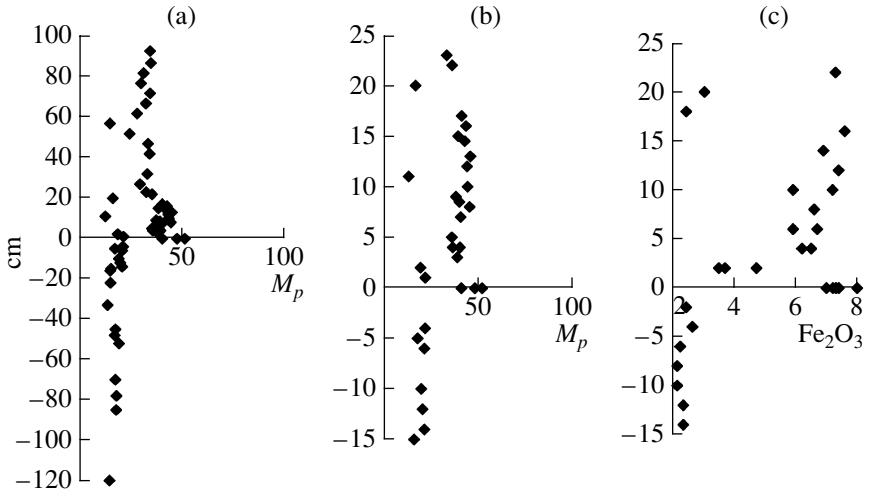

Fig. 10. Along-section behavior of (a, b) specific paramagnetic magnetization M_p and (c) total concentration of Fe_2O_3, wt % [Grachev et al., 2005].

the magnetic susceptibility (Figs. 1, 3, 10). Therefore, Fig. 10 reflects the iron distribution in the sediments studied; in general, this is also observable in Figs. 1a and 1b. Thus, the Maastrichtian and Danian deposits sharply differ in paramagnetic magnetization and magnetic susceptibility, i.e., in iron concentration, and the largest values of M_p are fixed in the interval 0–20 cm. The highest goethite concentrations (Fig. 3) are also obtained in this interval (in particular, in the **J** layer). Inside the **J** layer, the total iron concentration is highest at its base and decreases upward by a factor of ~2.5 (Table 1). Against the background of large values of M_p in the Danian rocks, the boundary layer **J** is distinguished by maximum values of M_p and χ and a series of interbeds have minimum values of M_p and χ (1–2 cm (**K** lens and t1), 11 cm (t7), 18–20 cm (**S**, **T**, and t12), 37 cm (t16), 57 cm (t20), and 77 cm (t24)). This suggests a certain rhythmicity (with a 10- and/or 20-cm periodicity) of drops in the iron accumulation in sediments. In the Maastrichtian deposits, where iron is distributed rather uniformly, the rhythmicity noted in the Danian layers is much more weakly expressed (Figs. 1, 10, 11).

Discussion of petromagnetic results. The following two levels of χ, M_{rs}, and M_s are well fixed in the section: (1) the weakly magnetic Maastrichtian marls underlying the **J** layer and the **K** lens and a series of interbeds in the Danian deposits and (2) more magnetic sandy–clayey deposits of the Danian (Table 1, Fig. 1). These two levels are generally consistent with the along-section distributions of magnetite (Fig. 8), goethite (Fig. 3), and paramagnetic magnetization (Fig. 10), i.e., with the total iron content in the rocks. This tendency is expressed to a lesser degree in the distribution of hemoilmenite (Fig. 6) and is absent in the distributions of titanomagnetite (Fig. 8) and metallic iron (Fig. 9). The aforementioned levels, primarily in the Danian part of the section, exhibit drops in the total iron content (expressed in the paramagnetic magnetization and magnetic susceptibility) that recur every ~10- and/or ~20-cm interval (Figs. 1, 10, 11). These intervals correspond to periods of ~10 and ~20 kyr, which is

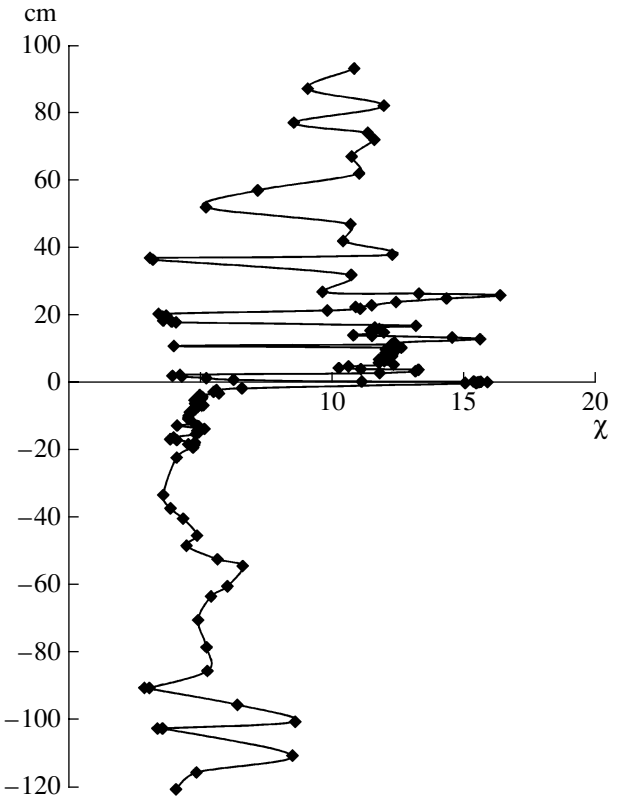

Fig. 11. Drops in the total iron concentration rhythmically recurring at approximately 10 and/or 18–20 cm periodicity that are expressed in terms of the magnetic susceptibility χ (10^{-9} m^3/kg).

close to the average precession period of the Earth's rotation axis and the main periods of the geodynamo [Merrill et al., 1996]. In the Maastrichtian part of the section, this rhythmicity is much less pronounced, which is apparently due to a very weak magnetization of the limestones.

With rare exceptions, the sediments under study are anisotropic and generally have a magnetic foliation, which points to a terrigenous nature of magnetic minerals. Many samples of the sandy–clayey rocks have an inverse magnetic fabric, with the maximum remanence or susceptibility perpendicular to the bedding plane. This is primarily associated with the presence of acicular goethite, in which an inverse magnetic fabric is inherent. Samples from the interbeds with small values of χ and M_p (in particular, from the **K**, **S**, and **T** layers) differ from the remaining samples by isotropy and a substantial increase in the amount of secondary magnetite appearing due to laboratory heating (Table 2). This means that such samples contain authigenic (isotropic) magnetic and paramagnetic minerals oxidizing upon heating, forming magnetite. Such a mineral can be, for example, pyrite. This pattern of layers with small values of χ and M_p emphasizes the cyclicity of the sedimentation process.

Judging from the coercivity spectra, the ensembles of magnetic grains are similar in all samples, somewhat differing in marls and sandy–clayey deposits, and are characterized by high coercivity values. An exception is the **J** layer, containing not only an ensemble of magnetic grains similar to that in high coercivity samples of sandy–clayey deposits but also magnetic grains with a lower coercivity (the maximum of the coercivity spectrum at 25–40 mT). The coercivity spectra of the studied rocks are primarily controlled by goethite grains. The low coercivity part of the spectrum for the layer **J** is most likely caused by grains of metallic nickel and an iron–nickel alloy.

The along-section distributions of goethite and magnetite are generally similar and mainly reflect a concurrent accumulation of these minerals that occurred under lithologic control. As noted above, the goethite concentration increases in a jumpwise manner, beginning with the layer **J**, whereas the magnetite concentration "lags behind" lithology variations: it is very low or vanishes in the Maastrichtian marls, and very small values are also observed in the **J** layer, t1, and the **K** lens; only beginning with the **L** layer, i.e., above the K/T boundary by 4 cm (later by about 4000 yr), does the magnetite concentration substantially increase, continuing to increase up to the **O** layer (Fig. 8).

The hemoilmenite concentration appreciably increases above the **J** layer, where the magnetite and goethite concentrations also increase but, higher along the section, the hemoilmenite concentration abruptly drops, as in the Maastrichtian limestones (Fig. 6), marking the zone of higher oxidation of ilmenite grains in the sediments. This is a zone of higher accumulation of goethite and magnetite.

The chaotic distribution of titanomagnetite is unrelated to both lithologic characteristics of the section and the K/T boundary (Fig. 8). Rather the titanomagnetite composition typical of basalts is associated with volcanic eruptive activity and eolian dispersal of titanomagnetite.

The along-section distribution of metallic iron is monotonically chaotic, and the scatter in its concentration, varying from 0.001 to 0.0015%, is within the uncertainty of the estimation of its magnetization contribution from the TMA curve. We relate the origin of metallic iron to cosmic meteoritic dust.

Against this general background, the **J** layer is sharply distinguished by anomalously high peaks of the paramagnetic magnetization and magnetic susceptibility. These peaks are caused by an anomalously high total iron content, first of all, in hydroxides, both paramagnetic and ferromagnetic (goethite); i.e., beginning with the **J** layer, accumulation of iron in the form of hydroxides increased in a jumpwise manner. This jump is confined to the base of the **J** layer (the first millimeters of its thickness). The concentration of hydroxides in the upper part of this layer decreases by about 2.5 times. However, the total content of magnetic minerals in the **J** horizon is similar to that in other horizons of the section (Fig. 1). The **J** layer differs from the remaining layers by the presence of nickel and an iron–nickel alloy. Their average concentration in the **J** layer does not exceed 0.005%. As noted above, metallic nickel and its alloy with iron are locally and very nonuniformly distributed across the **J** layer.

As noted in the Introduction, many researchers fixed the magnetic susceptibility peak at or near the K/T boundary in both epicontinental and marine–oceanic sediments. This peak occurs in two variants, depending on the lithologic type of the section: (1) if Maastrichtian carbonate deposits are overlain by Danian sandy–clayey sediments, a sharp peak of the susceptibility is observed in the boundary layer, whereas the susceptibility insignificantly decreases in the Danian sediments but still exceeds its value in the Maastrichtian layers (for example, this pattern is observed in the sections Gams (Austria), Teplovka (Volga region) [Molostovsky et al., 2006], and Kubalach (Crimea) [Yampolskaya et al., 2004], and (2) a sharp peak of susceptibility confined to the boundary clay layer is observed in carbonate deposits near the K/T boundary including a thin clayey interbed (the sections Koshak (Mangyshlak) [Pechersky et al., 2006], Tetritskaro (Georgia) [Adamia et al., 1993], and Abat (Oman) [Ellwood et al., 2003]). The majority of researchers are inclined to explain the χ peak as a result of terrigenous accumulation of magnetic minerals [Molostovsky, 1986; Ellwood et al., 2003; Yampolskaya et al., 2004; and others]. However, judging from the results of a comprehensive study of the Gams section presented in our paper, the main con-

tribution to the susceptibility is made by the paramagnetic magnetization, and this is characteristic of all aforementioned sections. Thus, an abrupt increase in the paramagnetic magnetization, primarily controlled by the content of iron hydroxides, is obviously common for the K/T boundary layers of all of the above sections. The paramagnetic magnetization in the boundary layer itself is highest in its lower part, where it attains 0.06 A m^2/kg (the Gams and Tetritskaro sections), and drops in its upper part by a factor of 2.5–3.

In all sections, goethite varies in nearly the same way as the paramagnetic magnetization. We may state that the goethite concentration and paramagnetic magnetization value were determined independently; therefore, such a correlation confirms the fact that the paramagnetic material primarily consists of iron hydroxides. Consequently, the enrichment in iron hydroxides, in both paramagnetic and weakly ferromagnetic forms, is a feature typical of the K/T boundary. Thus, only the enrichment in iron hydroxides can be considered as a global regular phenomenon associated with the K/T boundary. This phenomenon resembles the formation process of metal-bearing sediments and ferruginous micronodules as a result of volcanic and hydrothermal activities [Gurvich, 1998]. This process differs significantly from terrigenous accumulation of magnetic minerals. All remaining magnetic minerals reflect either the origin of these minerals (for example, cosmogenic balls of metallic iron and nickel or volcanogenic grains of titanomagnetite and ilmenite) or local conditions of accumulation of terrigenous material (for example, magnetite and ilmenite). A foliated magnetic fabric of sediments points to a detrital origin of both iron hydroxides and other magnetic minerals.

CONCLUSIONS

(1) Accumulation of iron hydroxides sharply increases at the K/T boundary, and this is most likely a global phenomenon unrelated to local physiographic conditions of accumulation of terrigenous material in sediments. The term "global" does not mean that iron hydroxides are *everywhere* accumulated at the K/T boundary. It means a widespread occurrence of this effect, both on land and in the ocean. This pattern is not inherent in the K/T boundary alone: iron hydroxides are accumulated in sediments not only at boundaries of geological eras; however, at the boundaries of geological eras, this phenomenon is regular.

(2) As distinct from iron hydroxides, other magnetic minerals accumulate variously, apparently depending on the origin of these minerals (for example, cosmogenic balls of iron and nickel or volcanogenic grains of titanomagnetite and ilmenite). The magnetic foliation of sediments is evidence for the detrital origin of iron hydroxides and other magnetic minerals.

(3) The base of the boundary layer **J** is enriched in titanomagnetite grains of volcanic origin. Coincidence of accumulation times of titanomagnetite and iron hydroxides possibly points to their common source; namely, titanomagnetite formed due to eolian dispersal and precipitation of products of volcanic eruptions, whereas iron hydroxides are products of the hydrothermal activity associated with the same volcanism. Note that an interval of eruptive activity is short, while the accumulation of iron hydroxides is a somewhat longer process.

(4) The jump in the accumulation of iron hydroxides in the boundary layer is unrelated to impact events. Thus, in the Gams section, indicators of an impact event (the presence of metallic nickel and its alloy with iron and an anomalous iridium concentration) are confined to the upper part of the **J** layer, whereas the jump in the accumulation of iron hydroxides and titanomagnetite is fixed at the base of this layer. Moreover, a sharp increase in the concentration of iron hydroxides is observed in all sections mentioned above, whereas metallic nickel is found in the Gams section alone. Enrichment in balls of cosmogenic metallic iron at the K/T boundary has been noted in none of the studied sections. Thus, direct indicators of an impact event at the K/T boundary are absent.

REFERENCES

1. *A Geological Time Scale*, Ed. by F. M. Gradstein et al. (Cambridge Univ. Press, Cambridge, 2004).
2. Sh. Adamia, N. Salukadze, M. Nazarov, et al., "Geological Events at the Cretaceous–Paleogene Boundary in Georgia (Caucasus)," Geol. Carpathica **23** (3), 35–43 (1993).
3. V. I. Bagin, T. S. Gendler, and T. A. Avilova, *Magnetism of α-Oxides and Hydroxides of Iron* (IFZ AN SSSR, Moscow, 1988) [in Russian].
4. B. V. Burov, D. K. Nourgaliev, and P. G. Yasonov, *Paleomagnetic Analysis* (KGU, Kazan, 1986) [in Russian].
5. S. C. Cande and D. V. Kent, "Revised Calibration of the Geomagnetic Polarity Time Scale for the Late Cretaceous and Cenozoic," J. Geophys. Res. **100**, 6093–6095 (1995).
6. R. Egli, "Analysis of the Field Dependence of Remanent Magnetization Curves," J. Geophys. Res. **108** (2003).
7. B. B. Ellwood, W. D. MacDonald, C. Wheeler, and S. L. Benoist, "The K–T Boundary in Oman: Identified Using Magnetic Susceptibility Field Measurements with Geochemical Confirmation," EPSI **206**, 529–540 (2003).
8. A. F. Grachev, O. A. Korchagin, H. A. Kollmann, et al., "A New Look at the Nature of the Transitional Layer at the K/T Boundary Near Gams, Eastern Alps, Austria, and the Problem of the Mass Extinction of the Biota," Russ. J. Earth Sci. **7** (2005).
9. R. Lahodynsky, "Lithostratigraphy and Sedimentology across the Cretaceous/Tertiary Boundary in the Flyschgosau (Eastern Alps, Austria)," Riv. Espanola Paleontol. No. Extraordinario, 73–82 (1988).
10. A. V. Lykov and D. M. Pechersky, "Stability Range of Magnetic Minerals in Basalts from Magnetometric

Data," Izv. Akad. Nauk SSSR, Fiz. Zemli, No. 12, 58–63 (1976).

11. A. V. Lykov and D. M. Pechersky, "Experimental Study of Magnetic Properties of Basalts in Relation to the Conditions of Their Formation," Izv. Akad. Nauk SSSR, Fiz. Zemli, No. 4, 65–74 (1977).
12. H. J. Mauritsch, "Der Stand der Palaeomagnetischen Forschung in den Ostaplen," Loebn. Hefte Angew. Geophys. **1**, 141–160 (1986).
13. R. T. Merrill, M. W. McElhinny, and P. L. McFadden, *The Magnetic Field of the Earth* (Academic, San Diego, 1996).
14. E. A. Molostovsky, "Scalar Magnetic Characteristics of Rocks as Indicators of Sedimentation Conditions," in *Use of Rock Magnetism in Geological Surveys*, Ed. by L. E. Sholpo, B. Sh. Rusinov, M. G. Ilaev, et al. (Nedra, Leningrad, 1986), pp. 58–73 [in Russian].
15. E. A. Molostovsky, V. A. Fomin, and D. M. Pechersky, "Sedimentogenesis in Maastrichtian–Danian Basins of the Russian Plate and Adjacent Areas in the Context of Plume Geodynamics," Russ. J. Earth Sci. **8** (2006).
16. T. Nagata, *Rock-Magnetism* (Maruzen, Tokyo, 1961; IL, Moscow, 1965) [in Russian].
17. D. M. Pechersky and A. V. Garbuzenko, "The Mesozoic–Cenozoic Boundary: Paleomagnetic Characteristic," Russian J. Earth Sci. **7** (2) (2005).
18. D. M. Pechersky, D. K. Nourgaliev, and Z. V. Sharonova, "Magnetolithologic and Magnetomineralogical Characteristics of Sediments at the Mesozoic/Cenozoic Boundary: The Koshak Section (Mangyshlak Peninsula)," Fiz. Zemli, No. 11, 99–112 (2006a) [Izvestiya, Phys. Solid Earth **42**, 957–970 (2006a)].
19. D. M. Pechersky, A. F. Grachev, D. C. Nourgaliev, et al., "Magnetolithologic and Magnetomineralogical Characteristics of Deposits at the Mesozoic/Cenozoic Boundary: Gams Section (Austria)," Russ. J. Earth Sci. **8** (3) (2006b).
20. C. Richter and B. A. van der Pluijm, "Separation of Paramagnetic and Ferrimagnetic Susceptibilities Using Low Temperature Magnetic Susceptibilities and Comparison with High Field Methods," Phys. Earth Planet. Inter. **82**, 111–121 (1994).
21. D. J. Robertson and D. E. France, "Discrimination of Remanence-Carrying Minerals in Mixtures, Using Isothermal Remanent Magnetization Acquisition Curves," Phys. Earth Planet. Inter. **82**, 223–234 (1994).
22. R. Rocchia, D. Boclet, Ph. Bonte, et al., "The Cretaceous–Tertiary Boundary at Gubbio Revisited: Vertical Extent of the Ir Anomaly," Earth Planet. Sci. Lett. **99**, 206–219 (1990).
23. L. E. Sholpo, *Rock Magnetism Applications to Geological Problems* (Nedra, Leningrad, 1977) [in Russian].
24. S. V. Vonsovskii, *Magnetism* (Nauka, Moscow, 1971) [in Russian].
25. O. B. Yampolskaya, M. V. Pimenov, V. A. Fomin, et al., "Magnetic Properties of Cretaceous–Paleogene Boundary Deposits in the Mountainous Crimea: Preliminary Results," in *Paleomagnetism and Magnetism of Rocks: Theory, Practice, and Experiment. Proc. Int. Symp.* (KGU, Kazan, 2004) [in Russian].
26. P. G. Yasonov, D. K. Nourgaliev, B. V. Bourov, and F. Heller, "A Modernized Coercivity Spectrometer," Geol. Carpathica **49** (3), 224–226 (1998).